Depopulation mechanisms of atomic hydrogen in the n=3 level following two-photon excitation by a picosecond laser

Corinne Y Duluard, Laurent Invernizzi, Khaled Hassouni, Guillaume Lombardi, Kristaq Gazeli, Swaminathan Prasanna

Depopulation mechanisms of atomic hydrogen in the n=3 level following two-photon excitation by a picosecond laser

Corinne Y. Duluard[1*], Laurent Invernizzi[1], Khaled Hassouni[1], Guillaume Lombardi[1], Kristaq Gazeli[1], Swaminathan Prasanna[1]

[1]Laboratoire des Sciences des Procédés et des Matériaux, LSPM, CNRS, Université Sorbonne Paris Nord, UPR 3407, F-93430 Villetaneuse, France

*corresponding author: corinne.duluard@lspm.cnrs.fr

Abstract

One of the major constraints of measurements of atomic hydrogen densities using Two-Photon Absorption Laser Induced Fluorescence (TALIF) in most plasma and combustion environments is the determination of fluorescence decay times ($\tau_{fluo\,H}$), especially when using nanosecond-lasers or slow acquisition systems. Therefore, it is necessary to identify the depopulation processes of the laser excited level in order to correctly estimate $\tau_{fluo\,H}$. In this study, depopulation mechanisms of atomic hydrogen excited by two-photon absorption to the n=3 level (H(n=3)) have been investigated using a picosecond-laser excitation and acquisition of fluorescence by a streak camera, which allowed for direct measurement of $\tau_{fluo\,H}$ and hence, the atomic hydrogen densities, in a H_2 microwave plasma operating in the pressure range 20-300 Pa. By combining these measurements with a detailed H(n=3) collisional radiative depopulation model, it was found that full mixing amongst the H(n=3) sub-levels occurs in our discharge conditions, even at a pressure as low as 20 Pa. Moreover, it is also seen that the Lyman β line is only partially trapped, as its escape factor Λ_{31} decreases from 0.94 – 0.98 down to 0.58 – 0.86 while the measured atomic hydrogen density rises from $8 \pm 5 \times 10^{19}\ m^{-3}$ to $9 \pm 6 \times 10^{20}\ m^{-3}$. This means that the radiative decay rate of H(n=3) atoms varies with pressure and the classical Stern-Volmer method used to determine the quenching cross-section of excited H(n=3) in collisions with H_2 molecules, $\sigma_{Q\,H(n=3)/H_2}$, is not valid for our measurements. We used two different physics-based approaches, and show that the quenching cross-section $\sigma_{Q\,H(n=3)/H_2}$ lies in the range $90 - 106 \times 10^{-20}\ m^2$, which can be averaged as $98 \pm 8 \times 10^{-20}\ m^2$. This substantially improved estimation of $\sigma_{Q\,H(n=3)/H_2}$obtained in this work will be useful for the accurate estimation of H(n=3) fluorescence decay times and therefore the atomic hydrogen densities.

1 Introduction

Atomic hydrogen is a key-species that plays a central role in a variety of plasma processes. This is especially the case for material synthesis, thin film deposition or surface treatments. Amongst the many examples reported in the literature we can cite diamond or hydrogenated amorphous carbon deposition [1]–[3], carbon nanostructures synthesis, e. g. graphene [4], silicon thin films deposition [5], [6], hexagonal boron nitride (h-BN) deposition [7]. In these processes, atomic hydrogen is usually responsible for the activation of the gas phase, e.g. methane dissociation, the stabilisation of the dangling bonds on the surface of growing deposits, e.g. diamond, silicon, and h-BN films, etching of undesirable phases, e.g. sp2 phases during diamond deposition, and reaction with the substrate

material. As a result, atomic hydrogen concentration is very often the major key plasma characteristic that governs the quality and the growth kinetics of the targeted materials in plasma processes. Atomic hydrogen may also be a central species in plasma processes used for chemical synthesis. This is for example the case in N_2/H_2 plasmas where atomic hydrogen plays a key-role in activating nitrogen in the form of highly reactive NH_x radicals [8], [9]; the activation efficiency of nitrogen is usually strongly linked to the ability of the plasma to dissociate hydrogen and subsequently to the atomic hydrogen concentration. Therefore, developing and optimising hydrogen-containing plasma processes and understanding the fundamental phenomena involved very often requires the knowledge of the space-time distribution of atomic hydrogen density. Usually atomic hydrogen shows a highly non-equilibrium behaviour even for thermal and high pressure plasmas and its density is very often much larger than what would be predicted on the basis of thermochemical equilibrium assumption [10], [11]. Therefore the estimation of atomic hydrogen density requires the development of sophisticated non-equilibrium plasma models that need to be validated by advanced diagnostics [12]. Unfortunately, measuring the absolute atomic hydrogen density can be highly challenging, especially when spatial resolution is required to account for temperature and density gradients in the vicinity of the plasma boundaries. Straightforward techniques based on optical emission spectroscopy such as actinometry give only access to the relative variation of the density [13] and a collisional radiative model is required for calibration [14], [15] which affects the robustness and accuracy of the method. Other techniques based on chemical titration such as NO_2 titration are very specific to post-discharge conditions and uniform concentration fields and are mainly suitable for calibration purposes [16], [17]. In fact, the only technique that in principle allows space and time-resolved measurements of atomic hydrogen density in plasmas is Two-Photon Absorption Laser Induced Fluorescence (TALIF).

Firstly introduced by Bokor *et al.* in 1981 [18], TALIF of atomic hydrogen using two-photon excitation to the n=3 electronically excited level, denoted H(n=3) hereafter, and subsequent detection of the fluorescence at 656.3 nm, became of increasing use in the combustion [19]–[25] and plasma communities [26]–[34] to monitor atomic hydrogen with a good spatial resolution.

To obtain absolute atomic density values, a calibration of the corresponding TALIF signal is required. The first calibration technique was based on NO_2 titration in a reference discharge flow reactor [16]. Then, a second technique makes use of the TALIF signal produced by a known density of krypton introduced separately in the same reactor [28], [29]. For both methods, the determination of the characteristic decay time of the atomic hydrogen fluorescence ($\tau_{fluo\,H}$) is necessary; the hydrogen densities extracted from TALIF measurements are indeed proportional to the fluorescence signal intensities and to the inverse of the fluorescence decay time when secondary phenomena are negligible.

Despite its apparent simplicity, one of the major bottlenecks of TALIF measurement of atomic hydrogen density is the difficulty to accurately estimate $\tau_{fluo\,H}$ in most plasma and combustion environments. Due to the collisional quenching of H(n=3) in these environments, $\tau_{fluo\,H}$ decreases with the rise in the densities of heavy species, and reduces to the order of a few nanoseconds for pressures as low as a few hundred pascals, which corresponds to the resolution limit of conventional

photomultiplier tubes. Even if one manages to use an acquisition system with sub-nanosecond resolution, it is complicated to estimate $\tau_{fluo\,H}$ when using a laser having a larger pulse duration such as that of a typical nanosecond laser (~10 ns). In other words, measurement of $\tau_{fluo\,H}$ for most laboratory conditions would only be feasible by using a combination of ultrafast lasers such as picosecond [22], [23], [35] or femtosecond [31] lasers and a fast acquisition system [22], [35].

Therefore, when $\tau_{fluo\,H}$ cannot be properly measured experimentally, one has to consider the whole collisional and radiative processes involved in the H-atom TALIF scheme to estimate its value [32]. However, the rather intricate depopulation kinetics of the H(n=3) state does not make this any simpler. According to the two-photon selection rules, both the 3s and 3d levels are populated by the two-photon absorption process. Collisions of excited H atoms with heavy particles not only induce the overall quenching of H(n=3), but also a mixing amongst the 3s, 3p and 3d levels. This mixing process can strongly impact the observed fluorescence signal and especially the corresponding radiative decay rate. As a matter of fact, the resulting population of the 3p level, from the photo-excited 3s and 3d levels *via* mixing induces an additional fluorescence to both the 2s and the 1s levels. Furthermore, the latter transition, i.e., the Lyman β line at 102.57 nm, is resonant and can be absorbed by the surrounding ground-state H atoms. As a result the Lyman β emission is, at least partly, trapped [36], [37]. Therefore, the collisional environment, i.e. temperature, pressure, atomic hydrogen density and the concentrations of the different quenchers of H(n=3), affects the observed fluorescence decay rate $1/\tau_{fluo\,H}$. Furthermore, the wide-range of collisional cross sections reported in the literature [20], [38] affects the estimation of the collisional decay rates. Therefore, it is essential to identify the right depopulation mechanisms, i.e. radiative and collisional processes, in order to determine the fluorescence decay rate accurately.

As collisional quenching of H(n=3) by H_2 molecules is very efficient, some authors have tried to experimentally measure these rate coefficients ($k_{Q\,H(n=3)/H_2}$) or cross sections ($\sigma_{Q\,H(n=3)/H_2}$) [19], [20], [28], [38], [39]. Such measurements were generally carried out using lasers with a nanosecond time-scale pulse width for the photo-excitation to H(n=3) [19], [20], [28], [38] followed by monitoring the 656.3 nm fluorescence line, in the pressure range 1-300 Pa. Likewise, these studies made use of different assumptions on the de-excitation kinetics of H(n=3) and thus the reported $k_{Q\,H(n=3)/H_2}$ or $\sigma_{Q\,H(n=3)/H_2}$ values are spread over a wide range ($65 \times 10^{-20}\ m^2$ [20] to $156 \times 10^{-20}\ m^2$ [38]).

The objective of this paper is twofold. Firstly, we will thoroughly analyse how the interplay between the different radiative and collisional processes mentioned above affects the H(n=3) fluorescence decay kinetics in a pure hydrogen plasma operating in the range 20 to 300 Pa. Secondly, this analysis will be extended to determine reliable values of the collisional quenching cross section $\sigma_{Q\,H(n=3)/H_2}$ while estimating the escape factor (denoted Λ_{31}) of the Lyman β line for the atomic hydrogen density range that characterises the investigated plasmas. These data are needed for estimating $\tau_{fluo\,H}$ which is necessary for the measurement of atomic hydrogen densities by the most widely used nanosecond-TALIF. For this purpose, we rely on TALIF measurements carried out using a picosecond laser and a streak camera. This allows reaching accurate values for the fluorescence

decay time without any complex model for the de-excitation process of H(n=3), and therefore measuring absolute atomic hydrogen density. Moreover, using a pure hydrogen plasma with weak dissociation (< 5%), the quenching of H(n=3) is essentially due to collisions with the H_2 molecule.

The present paper is organised as follows: in section 2 the methodology chosen for analysing the kinetics of H(n=3), and the experimental TALIF measurements are described. The results are presented in section 3 and discussed through a critical comparison with previously published data in section 4. The main conclusions are eventually summarised in section 5.

2 Method

2.1 Hydrogen n=3 excited level kinetics during the TALIF process

The excitation and de-excitation processes of the H(n=3) level involved during TALIF are depicted in Figure 1. Radiative processes are represented as full lines, while collisional processes are schematized by dotted lines.

Both the 3s $^2S_{1/2}$ and 3d $^2D_{3/2,\ 5/2}$ levels are populated by the two-photon absorption process, the two-photon cross section ratio $\sigma^2_{1s\rightarrow 3d}/\sigma^2_{1s\rightarrow 3s}$ being 7.56 [40]. When the laser intensity is kept low enough to prevent secondary phenomena such as photoionization and amplified spontaneous emission, the main processes that occur after the excitation of the 3s and 3d levels are:

- Radiative decay to the 2p level, along the Balmer α line at 656.3 nm; this is the detected fluorescence signal.
- Quenching due to collisions with H_2 molecules and H atoms with an average rate $Q_{H(n=3)}$ for the whole n=3 level.

Additionally, collisions of excited atomic hydrogen with heavy species lead to a redistribution of the population densities amongst the 3s, 3p and 3d levels. The mixing process contributes to the emission of radiation from the 3p level to both the 2s and the 1s levels. The resonant Lyman β line has a high probability to be absorbed by the surrounding 1s ground-state H-atom. The subsequent radiation trapping can be evaluated by an escape factor Λ_{31} whose value lies in the range 0 – 1. Λ_{31}=1 means full escape (i.e. no reabsorption of Lyman β transition), Λ_{31}=0 means full trapping (i.e. full reabsorption of Lyman β transition). The apparent emission coefficient of the Lyman β line is simply the product of the escape factor Λ_{31} and the Einstein coefficient for spontaneous emission, $A_{3p\rightarrow 1s}$.

Similarly to the assumption made by Preppernau *et al.* [41], we consider that, after its laser excitation, the depletion of the whole n=3 level can be simply described using a single collisional quenching rate $Q_{H(n=3)}$ (in s^{-1}) defined by:

$$Q_{H(n=3)} = k_{Q\ H(n=3)/H_2}\, n_{H_2} + k_{Q\ H(n=3)/H}\, n_H \qquad (1)$$

$k_{Q\ H(n=3)/H_2}$ and $k_{Q\ H(n=3)/H}$ represent the rate coefficients for the collisional quenching of H(n=3) by H_2-molecule and H-atom respectively. The relative importance of the two corresponding quenching routes is assessed in section 2.2.2.

Then, the population density equations for the three sub-levels 3s, 3p and 3d are, in the absence of secondary phenomena:

$$\frac{dn_{3s}}{dt} = R_{3s}(t) - \left(A_{3s\to 2p} + Q_{H(n=3)}\right)n_{3s}(t) + R_{ps} + R_{ds} - R_{sp} - R_{sd}$$

$$\frac{dn_{3p}}{dt} = -\left(A_{3p\to 2s} + \Lambda_{31}A_{3p\to 1s} + Q_{H(n=3)}\right)n_{3p}(t) + R_{sp} + R_{dp} - R_{ps} - R_{pd}$$

$$\frac{dn_{3d}}{dt} = R_{3d}(t) - \left(A_{3d\to 2p} + Q_{H(n=3)}\right)n_{3d}(t) + R_{sd} + R_{pd} - R_{ds} - R_{dp}$$

where $R_{3s}(t)$ and $R_{3d}(t)$ are the rates for laser excitation of levels 3s and 3d respectively, and $R_{ll'}$ are the rates of mixing for a transition from sub-level l to sub-level l' (l and l' being s, p and d of level n=3).

Adding the three equations for the individual sub-levels together, we get a lumped equation for the total density rate of H(n=3) as:

$$\frac{dn_3}{dt} = R_3(t) - (x_{3s}A_{3s\to 2p} + x_{3p}A_{3p\to 2s} + x_{3p}\Lambda_{31}A_{3p\to 1s} + x_{3d}A_{3d\to 2p} + Q_{H(n=3)})n_3(\mathrm{t})$$

with $n_3(t) = n_{3s}(t) + n_{3p}(t) + n_{3d}(t)$, $R_3(t) = R_{3s}(t) + R_{3d}(t)$ and x_{3s}, x_{3p} and x_{3d} the fractions $n_{3s}(t)/n_3(t)$, $n_{3p}(t)/n_3(t)$ and $n_{3d}(t)/n_3(t)$ respectively. Unsurprisingly, all the mixing terms disappear in the above equation as mixing amongst the three sub-levels has no effect on the total population of H(n=3).

The number of fluorescence photons emitted along the Balmer α line per unit time and per unit volume, i.e. the rate of emission of fluorescence photons per unit volume (in $m^{-3}s^{-1}$) can be formulated as:

$$\frac{dn_{photons}}{dt} = A_{3s\to 2p}n_{3s}(t) + A_{3p\to 2s}n_{3p}(t) + A_{3d\to 2p}n_{3d}(t)$$

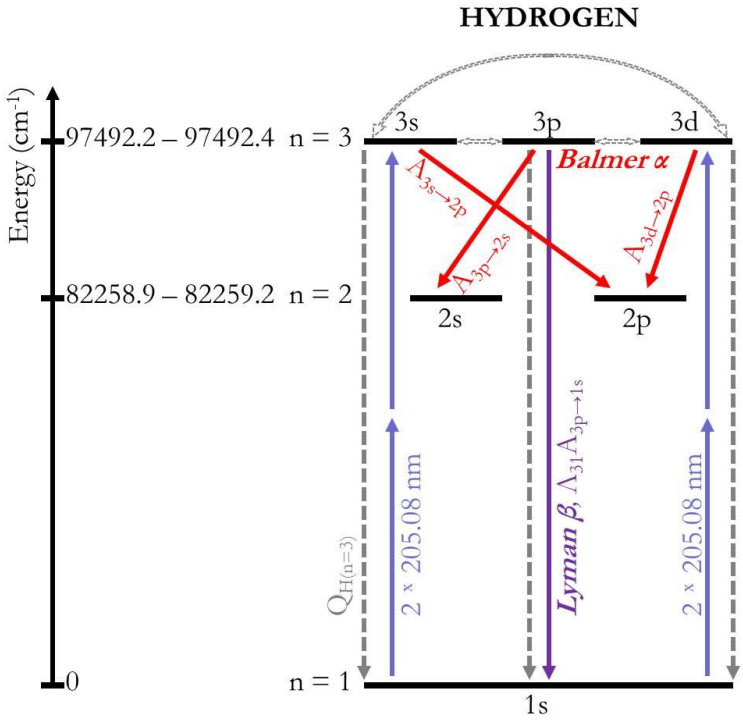

Figure 1 Excitation and de-excitation processes of the H(n=3) level taking place during TALIF. Radiative processes are represented as full lines, collisional processes (collisional mixing, collisional quenching) as dotted lines.

2.2 Determination of H(n=3) fluorescence decay rate

In this study, we examine the collisional and radiative de-excitation pathways of H(n=3) produced from the ground state by two-photon absorption, in a microwave H_2 plasma generated in the pressure range 20 – 300 Pa. The measured fluorescence decay rates of H(n=3) produced by two-photon excitation using a picosecond time-scale laser (10 ps pulse width) were compared to calculated values inferred from the collisional-radiative model schematized in Figure 1. We considered three different regimes.

In the first one the initial population distribution amongst the 3s and 3d levels is fully governed by their relative photo-excitation probabilities. This scenario is denoted hereafter “no mixing”. At this asymptotic limit, the 3p level is not populated and the Lyman β transition will be absent. As the populations of the two levels 3s and 3d decay independently, the fluorescence decay will be described by a double-exponential decay function. Physically, “no-mixing” is an asymptotic condition that would occur at extremely low pressures and in the absence of any electromagnetic field that may induce significant non-collisional mixing. For all practical operating conditions, mixing between the sub-levels is important to be considered.

The second regime, called “partial mixing” hereafter, occurs when mixing is not fast enough for the three sub-levels to assume statistical distribution. The time variation of the sub-level populations is more complex than an exponential decay, especially for the 3p level that is not initially populated by laser excitation, but only via mixing. In such a case, it is necessary to consider the three sub-levels individually and add up their contributions to the full fluorescence signal.

The last regime assumes a full mixing and an equilibrium population distribution of the 3s, 3p and 3d levels according to their statistical weights, i.e. $n_{3s}(t) = \frac{1}{9}n_3(t)$, $n_{3p}(t) = \frac{1}{3}n_3(t)$ and $n_{3d}(t) = \frac{5}{9}n_3(t)$. The three sub-levels mix over a time-scale that is much shorter than the fluorescence time-scale so as to ensure that the population distribution of the sublevels adjusts 'quasi-instantaneously' to their statistical weight. This necessarily entails that the population densities of 3s, 3p and 3d sub-levels will decay over time following the same decay rate as the whole population density $n_3(t)$. The time-variation of the whole n_3 level population density can therefore be described by the following relationship:

$$\frac{dn_3}{dt} = R_3(t) - \left[\left(\frac{1}{9}A_{3s\to 2p} + \frac{1}{3}A_{3p\to 2s} + \frac{5}{9}A_{3d\to 2s}\right) + \left(\frac{1}{3}\Lambda_{31}A_{3p\to 1s}\right) + Q_{H(n=3)}\right] n_3(t)$$

which is equivalent to:

$$\frac{dn_3}{dt} = R_3(t) - (A_{32} + \Lambda_{31}A_{31} + Q_{H(n=3)})n_3(t)$$

where $A_{32} = 4.41 \times 10^7\ s^{-1}$ is the average radiative decay rate of the Balmer α fluorescence line at 656.3 nm, $A_{31} = \frac{1}{3}A_{3p\to 1s} = 5.57 \times 10^7\ s^{-1}$ the average radiative decay rate of the Lyman β transition at 102 nm [42], and Λ_{31} the escape factor of the same emission line.

The number of fluorescence photons along the Balmer α line emitted per unit time and per unit volume thus reduces to:

$$\frac{dn_{photons}}{dt} = A_{32}n_3(t)$$

Hence the fluorescence decay after the end of the laser pulse is strictly mono-exponential with a characteristic decay time, the fluorescence decay time $\tau_{fluo\,H}$, which satisfies the following equation :

$$\frac{1}{\tau_{fluo\,H}} = A_{32} + \Lambda_{31}A_{31} + Q_{H(n=3)} = A_3 + Q_{H(n=3)} \quad (2)$$

A_3 is the total radiative decay rate (in s^{-1}) from the H(n=3) level.

It is noteworthy to mention that the trapping of the Balmer α line was neglected in this work since this line can be only absorbed by the much less populated H(n=2) electronically excited states. The estimation of the Lyman β line escape factor Λ_{31} in our experimental conditions is addressed in section 2.2.1. Further, three situations were considered depending on the assumption made on the value of the escape factor Λ_{31}. These correspond to a full mixing-full escape (FMFE), i.e., $\Lambda_{31} = 1$, full mixing-no escape (FMNE), i.e., $\Lambda_{31} = 0$, and full mixing-partial escape (FMPE), i.e., $0<\Lambda_{31}<1$. In the FMPE case, a pressure dependent escape factor Λ_{31} is calculated using measured absolute atomic hydrogen densities as discussed hereafter.

2.2.1 Estimation of the escape factor Λ_{31} for the Lyman β line

The influence of the resonant radiation absorption on the apparent de-excitation rate of a radiative source has been investigated by Holstein for a source assimilated to an infinite slab with a Doppler-broadened absorption line shape [36], and extended to the geometry of infinite cylinder, for several spectral line shapes [37]. The author studied the effect of resonant radiation trapping on the decay rate of excited state density after extinction of the excitation source. They proposed an asymptotic form of the escape factor (the so-called g factor in [36], [37]) for large optical depths by solving the radiative transport of excitation. In the field of plasma spectroscopy, the work of Holstein, and other authors [43] that later observed the decay of resonance lines and proposed other expressions for the escape factor, has been reviewed in great detail by Irons [44], [45].

The escape factor Λ depends on the absorption lineshape, the absorption coefficient k_0 at the centre of the absorption line, the source geometry, a length l that is characteristic of the shortest dimension of the source, and the spatial distribution of emitting atoms within the volume of the source.

In our pressure (20-300 Pa) and gas temperature (~600 K [46]) ranges, the 1s→3p absorption line profile is dominated by Doppler broadening. As a matter of fact, the corresponding Gaussian broadening is in the range $4.9 - 5.2 \times 10^{10}\ Hz$, which is more than 43 times larger than the sum of pressure and Stark broadening that are of the order of 1.1×10^{8} Hz (at 300 Pa, cf. p.299-300 in reference [47]) and at most 9.7×10^{8} Hz (cf. p.315 in reference [48], given the low electron density $\sim 5 \times 10^{17}\ m^{-3}$ with this type of plasma source [46]) respectively. In this case, the absorption coefficient $k^0_{1s\rightarrow 3p}$ (in m-1) in the centre of the H-atom 1s→3p absorption line may be expressed as follows (cf p.96-100 in reference [49]):

$$k^0_{1s\rightarrow 3p} = \frac{1}{8\pi}\sqrt{\frac{m_u Ar^0(H)}{2\pi k_B}}\frac{g_{3p}}{g_{1s}} A_{3p\rightarrow 1s}\,\lambda^3_{3p\rightarrow 1s}\frac{n_{H(1s)}}{\sqrt{T}} \qquad (3)$$

where $m_u = 1.660539 \times 10^{-27}\ kg$ is the atomic mass constant (p.50 in [50]), $Ar^0(H) = 1.008$ is the standard hydrogen atomic weight [51], k_B is the Boltzmann constant (in JK^{-1}), g_{3p} and g_{1s} are the degeneracies of the H 3p and 1s states respectively. $A_{3p\rightarrow 1s}$ is the Einstein spontaneous emission coefficient of the transition 3p→1s (in s^{-1}), and $\lambda_{3p\rightarrow 1s}$ the wavelength of the transition (in m). $k^0_{1s\rightarrow 3p}$ is proportional to the H-atom ground state density $n_{H(1s)}$ (in m^{-3}), which is assimilated to the atomic density n_H. It also depends on the inverse square root of the temperature of the H atoms, T (in K). Assuming a thermal equilibrium between H and H_2, the same temperature value was considered for both species, the determination of which is detailed in section 2.3.

We would like to emphasise that the source volume considered for the estimation of Λ_{31} is restricted to the interaction volume of the laser beam and the H_2 plasma. Plasma continuous emission at the same wavelength was filtered out by subtracting the background emission from the acquired pulsed signal intensity. Since the lens used for focusing the laser beam has a quite long focal length (350 mm), the beam diameter, measured to be ~250 µm in the centre of the reactor, is almost constant in the

fluorescence collection area. The collection optics images the fluorescence radiation to the entrance slit of a streak camera placed perpendicularly to the laser beam, with a magnification of 1. We thus approximated the source as an infinite cylinder of radius 125 µm for the calculation of Λ_{31} (cf figure 2).

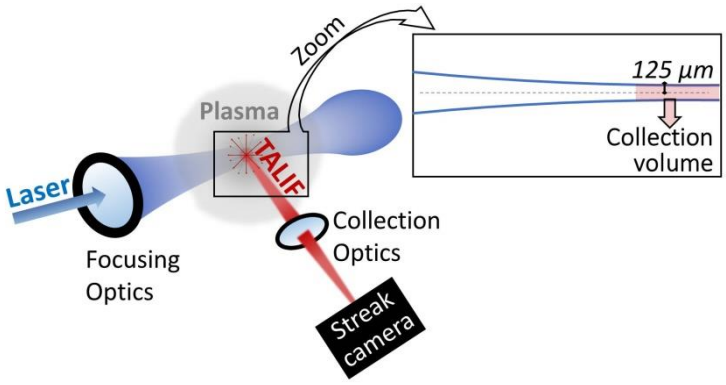

Figure 2 - Schematics of the TALIF experimental set-up, showing the collection volume of fluorescence considered as the source volume for the estimation of the escape factor Λ_{31}

Taking this radius as the characteristic length of absorption, the optical depth in the centre of the absorption line, defined as $\tau^0_{1s\rightarrow 3p} = k^0_{1s\rightarrow 3p} l$, increases from 0.04 to 0.44 as the atomic hydrogen density measured rises with pressure. Such values are too low for the application of Holstein's asymptotic formulation of Λ_{31}, which is considered valid for optical depths greater than 3. Amongst the formulations reviewed in [44], [45], we chose to apply the following empirical expression derived by Mewe for Doppler-broadened line assuming a spatially-uniform excitation [43], i.e. uniform distribution of excited atoms within the source :

$$\Lambda_{31} = \frac{2 - exp\left(-10^{-3}\tau^0_{1s\rightarrow 3p}\right)}{1 + \tau^0_{1s\rightarrow 3p}} \qquad (4)$$

Equation (4) was found to be accurate within 25% for both optically thin and optically thick media ($\tau^0_{1s\rightarrow 3p}$ in the range $0 - 10^4$).

2.2.2 Estimation of the collisional quenching rate

For each of the four scenarios mentioned previously, the fluorescence decay rate was calculated assuming a single collisional quenching rate $Q_{H(n=3)}$ for the whole H(n=3) level. We considered the quenching by both H_2-molecule and H-atom. The overall quenching rate is therefore given by:

$$Q_{H(n=3)} = k_{Q\ H(n=3)/H_2}\, n_{H_2} + k_{Q\ H(n=3)/H}\, n_H$$

The gas temperature T_{gas} was estimated (cf section 2.3) and a temperature-independent collisional cross section $\sigma_{Q\ H(n=3)/H_2}$(m^2) was formulated according to the relationship:

$$k_{Q\ H(n=3)/H_2} = \sigma_{Q\ H(n=3)/H_2} v_{th\ H(n=3)/H_2}$$

$v_{th\ H(n=3)/H_2}$ is the thermal velocity, defined by: $v_{th\ H(n=3)/H_2} = \sqrt{\frac{8k_B T_{gas}}{\pi \mu_{H(n=3)/H_2}}}$

with k_B the Boltzmann constant and $\mu_{H(n=3)/H_2}$ the reduced mass of the collision pair $H(n=3)/H_2$.

Finally, the collisional quenching rate is expressed as:

$$Q_{H(n=3)} = \sigma_{Q\ H(n=3)/H_2} v_{th\ H(n=3)/H_2} n_{H_2} + \sigma_{Q\ H(n=3)/H} v_{th\ H(n=3)/H} n_H \quad (5)$$

The quenching by atomic hydrogen mainly leads to associative ionisation reaction [52], the cross-section of which ($3.8 \times 10^{-20}\ m^2$ [52]) is 17 to 41 times lower than the collisional cross-section values published for the collisional-quenching of H(n=3) by H_2 molecules [20], [38], [39]. Furthermore, anticipating the results, a fairly moderate dissociation degree, i.e., typically below 5%, is expected for the investigated discharge conditions. As a result, collisional quenching of H(n=3) is largely dominated by the collision with H_2-molecule and depends almost exclusively on the H_2 density. This was estimated from total density (determined from the ideal gas law, through pressure monitoring and gas temperature measurements), and atomic hydrogen absolute densities obtained from calibrated picosecond TALIF measurements.

2.3 Experimental details and measurements

H atoms were generated in a H_2 microwave (MW) plasma in the 20-300 Pa pressure range using a commercial source (Sairem Hi-Wave). The MW power was supplied through a coaxial feed from a solid-state MW generator (Sairem GMS 200) that delivers a maximum power of 200 W. The operating MW frequency was tuned between 2.4 and 2.5 GHz in order to achieve optimal impedance matching between the source and the discharge system. The chamber, described in detail in [53], consisted of a 100 mm diameter stainless-steel six-way cross, the plasma source being placed at the top of the cross. Three flanges were dedicated to optical viewports. The laser beam crossed the plasma reactor through two fused silica viewports (90% transmission at 205 nm). The fluorescence was collected perpendicularly to the laser beam through a borosilicate viewport. The vacuum was obtained using a turbo-molecular pump (Edwards EXT75DX) assisted by a rotary pump (Pfeiffer Duo 6M), allowing a residual pressure of 10^{-5} Pa to be achieved. The working pressure in the chamber was manually adjusted by a diaphragm valve, and monitored using a capacitive gauge (Pfeiffer CCR363) working in the range 0.133–1333 Pa. The gases were injected in the reactor using mass flow controllers (Bronkhorst EL flow), the hydrogen gas flow rate being set at 5 sccm.

TALIF measurements on atomic hydrogen were performed using a picosecond tunable laser (EKSPLA® composed of three units: PL3140, APL2100 and PG411, pulse width of ~10 ps [54]. The laser excitation wavelength was tuned to the H $1s \rightarrow 3s$ and $1s \rightarrow 3d$ transitions at 205.08 nm and the fluorescence signal at 656.3 nm (Hα line) was observed. The laser light was guided and focused in the plasma reactor using a quartz lens with a 350 mm focal length. The fluorescence was collected at 90° by a set of quartz lenses which imaged the light to the slit of a streak camera (HAMAMATSU® C10910-05), in front of which an interference filter centred at 655 nm (Semrock FF01-655/15-25) was positioned.

The laser beam diameter at the measurement location was experimentally determined to be ~250 µm. The laser energy was manually adjusted by adding one or several neutral density filters after the output of the laser unit, and monitored with a joulemeter located at the end of the optical path [35].

The absolute atomic hydrogen densities were determined through calibration of H-atom fluorescence signal intensities with TALIF measurements on Kr atoms, introduced independently in the same reactor at a known pressure [3]. For these calibration measurements, the laser excitation wavelength was tuned to the Kr $4p^6 \quad {}^1S_0 \rightarrow 5p' \, [3/2]_2$ at 204.13 nm, and the fluorescence signal at 587.09 nm was observed using an interferential filter centred at 586 nm (Semrock FF02-586/15-25) in front of the streak camera.

For both H and Kr TALIF measurements, the laser energy density was kept low enough to limit the onset of secondary effects such as amplified spontaneous emission and photoionisation. This was assessed experimentally by working in the laser-energy domain providing a quadratic dependence of the fluorescence intensity on the laser energy, i.e., the so-called quadratic regime [55]. It was also verified that photodissociation of H_2 molecules by the laser was insignificant in this energy domain, as no TALIF signal was detected when the chamber was filled with H_2 gas and the plasma was turned off. Most measurements were thus performed with an energy in the range 10-12 µJ. Regarding Kr, the quadratic regime of excitation was limited to laser energies below 0.85 µJ at a pressure of 1000 Pa; this pressure (set by filling the reactor with Kr gas after closing the valve and switching off the pumping) was selected to keep high enough values of the signal-to-noise ratio.

The fluorescence decay times of H(n=3) atoms extracted from TALIF measurements served two purposes: to determine the atomic hydrogen absolute densities in conjunction with measured time-integrated fluorescence signal intensities, and to study the de-excitation pathways of H(n=3) atoms. We developed an algorithm that fits the measured fluorescence signal to the convolution of a theoretical TALIF signal and a Gaussian apparatus function [35].

Optical emission spectroscopy measurements were carried out on the H_2 plasma in various pressure and power conditions. The rotational temperature of H_2 molecules in the ground $X^1\Sigma_g^+, v = 0$ vibronic state was inferred from the emission of the Fulcher-α (2-2)Q band system, which is a reliable method for the range of pressures used in this study [56], [57]. It was observed that the rotational temperature mostly depended on the plasma source power, and a statistical analysis on the various measurements gave, for the plasma conditions used for the present paper, i.e. a fixed input power of 200 W, a rotational temperature of 595 ± 35 K. Owing to such low temperatures and to the picosecond laser linewidth, it was not possible to measure the temperature of atomic hydrogen using Doppler broadening of the 1s→3s, 3d two-photon absorption line profile. However, for plasma conditions considered in this study, one would expect the degree of non-equilibrium between the rotational and kinetic modes as well as between H and H_2 to be small and therefore one can assume thermal equilibrium between the rotational and kinetic modes of H_2 molecule, and also a thermal equilibrium between H and H_2. The latter assumption is further justified for the low dissociation degrees and the pressure range encountered in the present study, as shown by the Monte Carlo simulations of Tomasini

et al.[58]. Thus the total gas density was determined from the equation of state for perfect gas, using the rotational temperature of H_2 molecules inferred from the H_2 Fulcher-α emission band.

3 Results

3.1 Determination of atomic hydrogen densities and fluorescence decay rates

Calibrated TALIF measurements on atomic hydrogen were carried out in H_2 microwave plasma for pressures in the range 20-300 Pa. The absolute atomic hydrogen densities determined in this work are depicted in Figure 3(a) by a purple line with square symbols. They range between $(\sim 8 \pm 5) \times 10^{19}\ m^{-3}$ and $(\sim 9 \pm 6) \times 10^{20}\ m^{-3}$ in the investigated pressure range. The relative uncertainty on these values, pictured as a purple-shaded area, is of approximately 62 % and was calculated using the uncertainty propagation technique for independent variables. When possible, relative uncertainties of the variables were estimated during the experiments (pressure, transmission of windows), otherwise they were taken from manufacturers data (transmission of filters, quantum efficiency of detector) or from published physical data (spontaneous emission coefficients, two-photon excitation cross sections). As in reference [53], the major source of uncertainty came from the ratio $\sigma_{Kr}^{(2)}/\sigma_{H}^{(2)}$ of the Kr and H two-photon excitation cross sections, which was determined with an uncertainty of 50 % [28]. The second contribution came from the uncertainty on the Kr emission coefficient at the fluorescence wavelength 587.09 nm, 20 % [59].

The atomic density is seen to increase almost linearly in the pressure range 20 - 225 Pa and to remain practically constant for higher pressures. Despite this density increase, the atomic hydrogen fraction (blue line with circles in Figure 3(a)) shows a significant decrease with pressure. This decrease is especially marked above 225 Pa and the average atomic fraction values remain lower than 3 % in the highest range of pressures. These trends would indicate a smaller power density deposited in the plasma, which limits the enhancement of the dissociation rate at high pressure.

The fluorescence signal decays were at best fitted by a single exponential decay. Indeed, we do not identify the existence of multi-exponential components describing the decaying phase of the TALIF signal, which would allow us to distinguish the decay of each of the levels 3s, 3p and 3d in any of our experiments. The measured fluorescence decay rate $1/\tau_{fluo\,H}$ of excited H(n=3) is presented in Figure 3(b). It increases from $\sim 1.0 \times 10^{8}\ s^{-1}$ to $\sim 2.1 \times 10^{8}\ s^{-1}$ as the pressure rises from 20 to 300 Pa. The uncertainty on the experimental decay rate was calculated from the uncertainty on the characteristic decay time of the fluorescence, which was estimated at approximately 0.3 ns. The fluorescence decay rate remains nearly constant in the pressure range 20 – 60 Pa, and then almost linearly increases in the highest range of pressures.

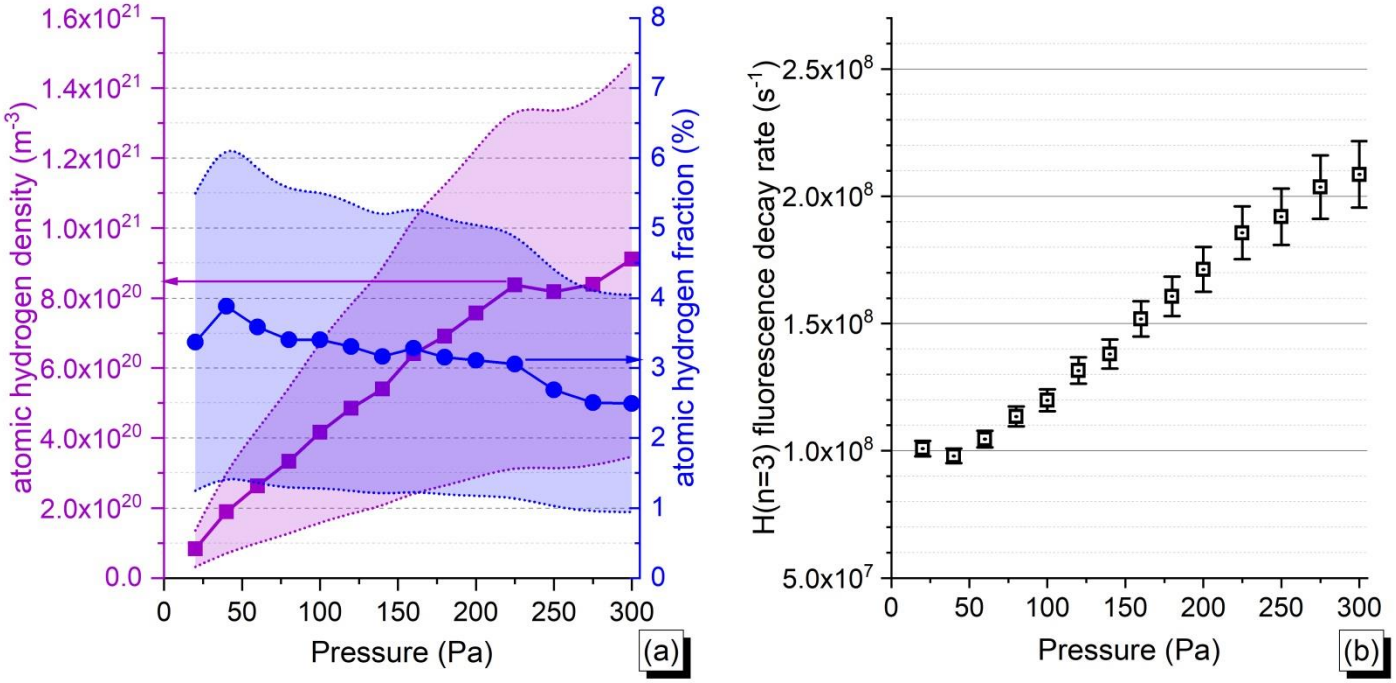

Figure 3 Measured atomic hydrogen densities, atomic hydrogen fractions (a) and H(n=3) fluorescence decay rates (b) as a function of H_2 plasma pressure.

3.2 Lyman β escape factor Λ_{31}

The measured atomic hydrogen density values were used to estimate the escape factor Λ_{31} of the Lyman β line, using equation (4) and assuming a 125 µm-radius infinite cylinder source. The corresponding values of Λ_{31} are plotted in Figure 4. More precisely, the blue line with blue diamonds corresponds to Λ_{31} values calculated using the hydrogen density values represented by purple squares in Figure 3(a). The blue-shaded area surrounding the blue line represents the uncertainty on Λ_{31} as inferred from the uncertainty on atomic hydrogen density. Whatever the formulation used to express Λ_{31} as a function of $\tau^0_{1s\rightarrow 3p}$ [37], [43]–[45], the escape factor decreases when increasing the absorber density. Since the relationship between Λ_{31} and $\tau^0_{1s\rightarrow 3p}$ is not linear, the upper and lower limits that determine the uncertainty on Λ_{31}were calculated using, for each pressure value, the lower and upper hydrogen densities, respectively. As such, the gap between the blue line with markers and the upper and lower limits of the shaded area is asymmetrical. From these calculations, Λ_{31} is close to 1 (0.94 – 0.98) at the lowest pressure, and decreases down to 0.58 – 0.86 at 300 Pa. Therefore, it appears that the Lyman β line is almost always partially trapped for the atomic hydrogen density range met in our plasmas. This is why, assuming full or no escape of Lyman β radiation in the investigation of the fluorescence decay rate is not valid for the studied range of atomic hydrogen densities.

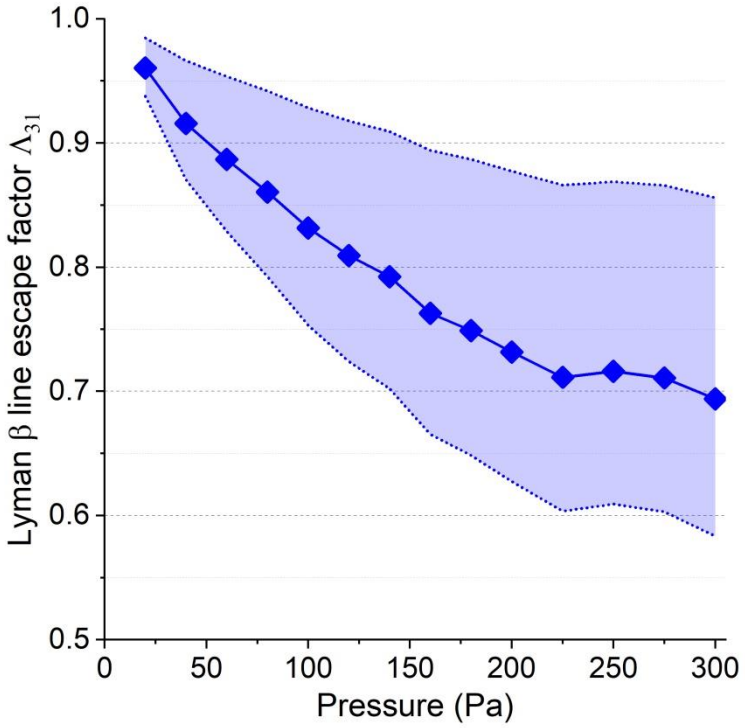

Figure 4 Calculated escape factor Λ_{31} (equation (4)) of the Lyman β line emitted following two-photon laser absorption from hydrogen ground state and complete mixing.

3.3 Comparison of experimental fluorescence decay rates with model predictions

The purpose of this section is to compare the experimental fluorescence decay rates with model results that use different values of $\sigma_{Q\,H(n=3)/H_2}$ proposed in the literature. The measured values of the fluorescence decay rate of H(n=3) atoms are compared in Figure 5 to those predicted by the model according to the two asymptotic conditions considered in this work, i.e. "no mixing", and "full mixing" with three different scenarios: FMNE, FMPE and FMFE as described in section 2.2. For the "no mixing" condition, the fluorescence signal intensity is largely dominated by the fluorescence emitted from the 3d level, due to the two-photon cross section ratio $\sigma^2_{1s\to 3d}/\sigma^2_{1s\to 3s}$ of 7.56 [40], and to the ratio $A_{3d\to 2p}/A_{3s\to 2p} = 10.24$ [42]. As a consequence, the apparent fluorescence decay rate for the "no-mixing" scenario is close to the fluorescence decay rate of the 3d level. The fluorescence decay rate in this scenario was therefore approximated by the fluorescence decay rate of the 3d level solely, for which the radiative decay rate is $A_{3d\to 2p} = 6.47 \times 10^7 s^{-1}$ [42].

Λ_{31} is calculated using equation (4), and two extreme values of $\sigma_{Q\,H(n=3)/H_2}$ proposed in the literature that differ by a factor 2.4 are used : (a) $156 \times 10^{-20}\ m^2$ [38], and (b) $65 \times 10^{-20}\ m^2$ [20].

Please note that the uncertainty range calculated for each scenario is represented as a coloured shaded area. The main contribution to the relative uncertainty of $Q_{H(n=3)}$ was the uncertainty on the temperature (595±35 K), which entailed relative uncertainties on the total gas density (6 – 12 %), the H_2 density (6 – 12 %), and the thermal velocity (3 %).

The major conclusions that can be drawn from the plots in Figure 5 are as follows: firstly, whatever the scenario chosen, the decay rate values predicted by the model using $\sigma_{Q\,H(n=3)/H_2} = 156 \times 10^{-20}\ m^2$

(Figure 5(a)) largely exceed the experimental values for pressures larger than 140 Pa. Inversely, the decay rate values predicted by the model using $\sigma_{Q\,H(n=3)/H_2} = 65 \times 10^{-20}\ m^2$ (Figure 5(b)) are lower than the experimental decay rates for pressures beyond 240 Pa. Also, it is noticeable that with the latter value of $\sigma_{Q\,H(n=3)/H_2}$ the measured decay rate values are in good agreement with the FMPE scenario, with pressure-dependent Λ_{31}, in the pressure range 80 – 140 Pa. For higher pressures the experimental data are in a better agreement with the FMFE scenario, i.e. $\Lambda_{31} = 1$. This would mean that the escape factor of the Lyman β line actually rises with pressure, which is unphysical. As a matter of fact, since the atomic hydrogen density increases with pressure, the escape factor Λ_{31} should decrease with this parameter. Therefore, the value of $65 \times 10^{-20}\ m^2$ is probably too small.

Moreover, it is interesting to notice that, for both values of $\sigma_{Q\,H(n=3)/H_2}$ tested, the experimental decay rate measured at a pressure of 20 Pa is closer to the values assuming full mixing amongst the 3s, 3p and 3d states and a rather high value of Λ_{31}. This result is consistent with the fairly low atomic hydrogen density, and the observed agreement would support a fast mixing amongst the 3s, 3p and 3d states even at low pressure. In fact, this result is in agreement with [27] who observed that full mixing amongst the 3s, 3p and 3d states occurs at pressures as low as 2 Pa.

It appears therefore that the emission of the Lyman β line and the variation of its escape factor Λ_{31} as a function of the atomic hydrogen density, and thus the pressure, need to be taken into account. The collisional quenching cross section values from the literature used in figure 5 (a) and 5 (b) are either too large or too small to obtain a good agreement between the measured and predicted fluorescence decay rate values. In the next section, our aim is to determine a more accurate value for the collisional quenching cross-section $\sigma_{Q\,H(n=3)/H_2}$ using two rather classical approaches and a more novel method.

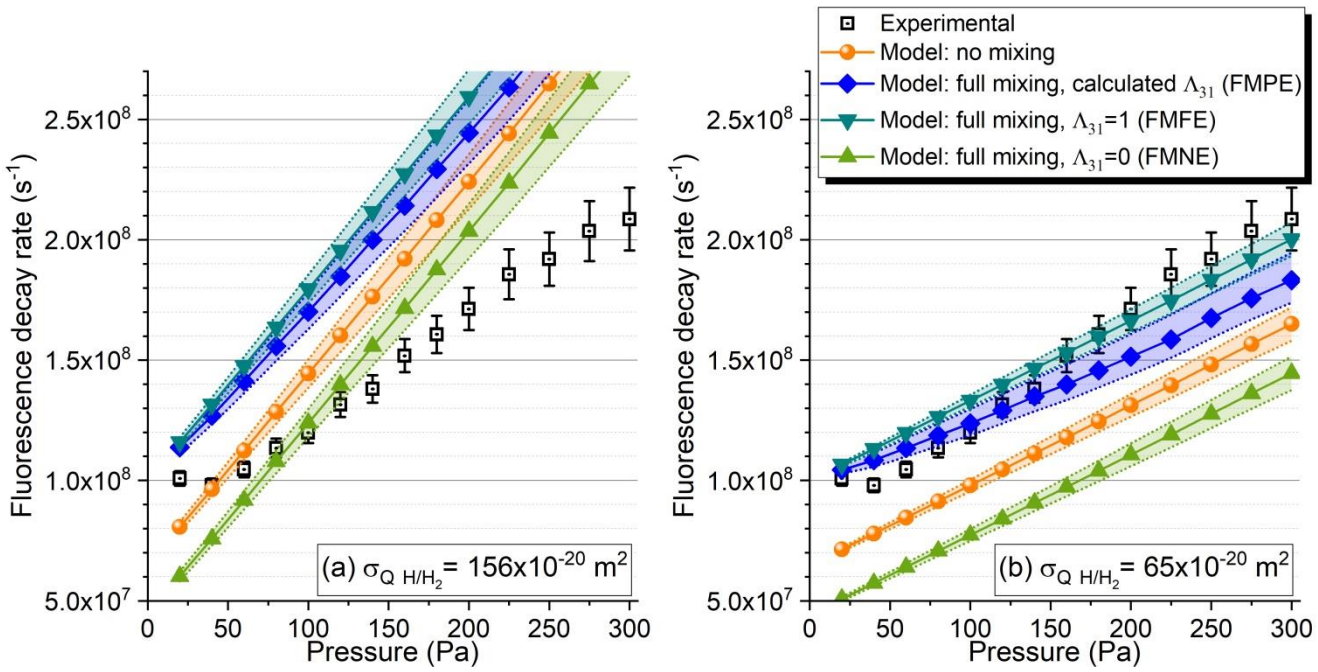

Figure 5 Comparison of experimental fluorescence decay rate of H(n=3) atoms with model predictions according to different scenarios, for (a) $\sigma_{Q\,H(n=3)/H_2} = 156 \times 10^{-20}\ m^2$, and (b) $65 \times 10^{-20}\ m^2$

3.4 Determination of the collisional cross section $\sigma_{Q\,H(n=3)/H_2}$

Usually, the collisional quenching cross-section value is determined using a Stern-Volmer plot, where the variation of the fluorescence decay rate as a function of the density of quenchers is fitted by a linear function. The slope of this function is the collisional quenching rate coefficient $k_{Q\,H(n=3)/H_2}$ and the intercept is the radiative decay rate. This procedure was applied to the case of the H(n=3)/H_2 collisional quenching using the variation of the fluorescence decay rate as a function of the density of molecular hydrogen, inferred from figure 3(b). The cross section value obtained in this way is approximately $85 \times 10^{-20}\ m^2$, which is in between the values reported by [20] and by [38]. Actually, the variation of the fluorescence decay rate as a function of the pressure in figure 3(b) shows a peculiar behaviour in the low-pressure domain, i.e., p< 60 Pa, where the decay rate does not vary linearly with the pressure. Moreover, since the escape factor Λ_{31} varies significantly in the range of pressures studied, the radiative decay rate is not constant in the conditions of interest making the Stern-Volmer approach to measure radiative decay rates and collisional cross-sections questionable.

Another physics based approach is discussed below that allows determining the quenching cross-section $\sigma_{Q\,H(n=3)/H_2}$ from the measured fluorescence decay rate, by taking into account the constraints on the escape factor and the trend of its variation with pressure as shown in figure 4.

Equations (2) and (5) enable expressing an effective escape factor $\Lambda_{31\,eff}$ as a function of the measured fluorescence decay rate $1/\tau_{fluo\,H\,exp}$ as follows:

$$\Lambda_{31\,eff} = 1/A_{31}\left(1/\tau_{fluo\,H\,exp} - A_{32} - \sigma_{QH(n=3)/H_2} v_{thH(n=3)/H_2} n_{H_2} - \sigma_{Q\,H(n=3)/H} v_{th\,H(n=3)/H} n_H\right) \quad (6)$$

Equation (6) shows that the effective escape factor values essentially depend on the pressure through H_2-density, on the measured fluorescence decay rate, and on the value adopted for $\sigma_{Q\,H(n=3)/H_2}$.

In Figure 6, $\Lambda_{31\,eff}$ variations as a function of the pressure are plotted for four values of $\sigma_{Q\,H(n=3)/H_2}$. This graph helps identifying the values of $\sigma_{Q\,H(n=3)/H_2}$ that are physically acceptable. The effective escape factor has indeed to satisfy two conditions: (i) its value is necessarily in the range 0 – 1, and (ii) it necessarily decreases with rising pressure, in agreement with increasing atomic hydrogen densities.

The first condition was evaluated using the average values of $\Lambda_{31\,eff}$ estimated at each pressure. Assuming a uniform probability distribution over the uncertainty range, this choice means that a cross-section value is rejected when it results in a value greater than 50% for the probability to find $\Lambda_{31\,eff}$ outside the interval [0, 1].

The second condition was evaluated considering the whole range of possible $\Lambda_{31\,eff}$ values, that are determined by the measurement uncertainties on the gas temperature, and $1/\tau_{fluo\,H\,exp}$, at each pressure. In this way, we excluded the $\sigma_{Q\,H(n=3)/H_2}$ values for which the upper limit of $\Lambda_{31\,eff}$ would be larger at higher pressure than at 20 Pa.

As such, the value of $156 \times 10^{-20}\ m^2$ [38] is too large, inducing a negative average value of $\Lambda_{31\,eff}$ for pressures above 100 Pa. The value $65 \times 10^{-20}\ m^2$ [20] is on the contrary too low since it implies an average value of $\Lambda_{31\,eff}$ greater than 1 for pressures above 180 Pa (cf. figure 6), and moreover an increase in $\Lambda_{31\,eff}$ with pressure. This is not physical as $\Lambda_{31\,eff}$ should decrease with the rise in pressure/atomic hydrogen density. Therefore, the correct cross-section value should be between the two reported values. The cross-section values that fulfil the two conditions are in the range $90 - 106 \times 10^{-20}\ m^2$; the $\Lambda_{31\,eff}$ values calculated for these two boundaries are also plotted in figure 6 for comparison.

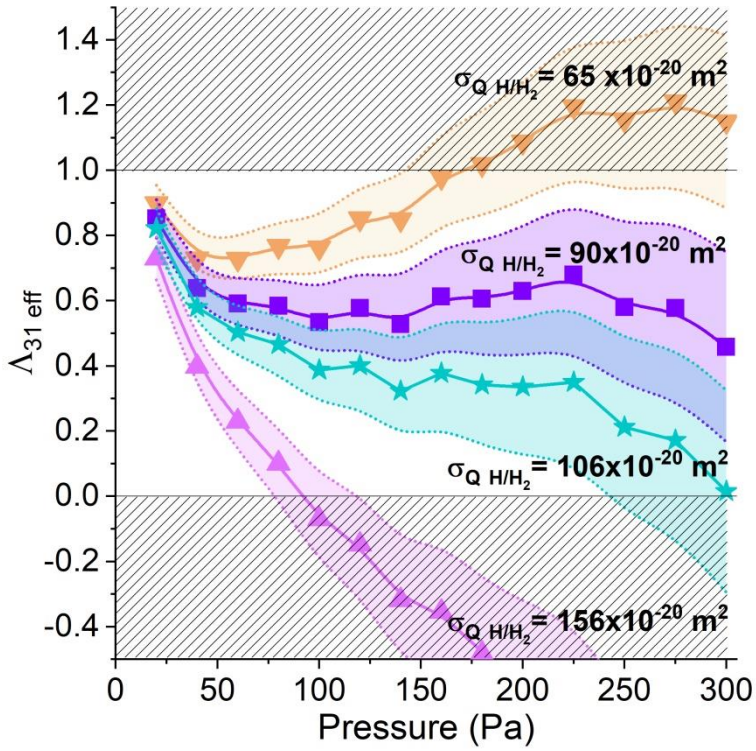

Figure 6 Effective escape factor $\Lambda_{31\,eff}$ calculated for several values of $\sigma_{Q\,H(n=3)/H_2}$

The value of $\sigma_{Q\,H(n=3)/H_2}$ can be also determined from a least square curve fit of the measured fluorescence decay rate as a function of pressure by equation (2) (where the collisional quenching rate is given by equation (5)). This method makes use of the estimated value of the escape factor Λ_{31} discussed in section 3.2 for the FMPE scenario. The other variables involved in the curve fitting procedure (escape factor Λ_{31}, molecular and atomic hydrogen densities, thermal velocities) are those previously determined for each pressure value. The $\sigma_{Q\,H(n=3)/H_2}$ value that minimises the gap between the fitting curve and the measured fluorescence decay rate is $80.8 \pm 2.5 \times 10^{-20}\ m^2$, which is slightly below the lower end of the acceptable range defined beforehand.

Figure 7 pictures the measured values of the fluorescence decay rate of H(n=3) atoms along with those predicted by the model according to the four scenarios already considered, for $\sigma_{Q\,H(n=3)/H_2} = 80.8 \times 10^{-20}\ m^2$. This value leads to a much better agreement between the FMPE scenario and the experimental data compared to the cross section values taken from literature (cf. figure 5). Despite this improvement, we believe that the value of $80.8 \times 10^{-20}\ m^2$ underestimates the actual value of

$\sigma_{Q\,H(n=3)/H_2}$ and that it is very likely in the range $90 - 106 \times 10^{-20}\ m^2$ as determined from the more robust physical constraints on the variation of the escape factor with pressure. As a matter of fact, a discrepancy still exists in the pressure range 40 – 100 Pa between the fluorescence decay rates measured experimentally and those calculated in the FMPE scenario with a $\sigma_{Q\,H(n=3)/H_2}$ value of $80.8 \times 10^{-20}\ m^2$. We believe that this discrepancy along with the slight underestimation of $\sigma_{Q\,H(n=3)/H_2}$ originate from an overestimation of the value of Λ_{31} determined using equation (3). A full treatment of the radiative transport of excitation in the rate equation describing the H(n=3) densities would certainly improve the fit between the model and the experimental data. Nevertheless, the fluorescence decay rate measured at 20 and 40 Pa is consistent with a fast mixing process amongst the 3s, 3p and 3d states, and in agreement with [27]. Further, the fluorescence decay rate predicted by the model using this approximated value of Λ_{31} is in rather good agreement, and even in very good agreement for pressures above 100 Pa, with the measurements.

The discussion above shows that the quenching cross-section $\sigma_{Q\,H(n=3)/H_2}$ lies in between $90 \times 10^{-20}\ m^2$ and $106 \times 10^{-20}\ m^2$, with a mean value of $98 \times 10^{-20}\ m^2$.

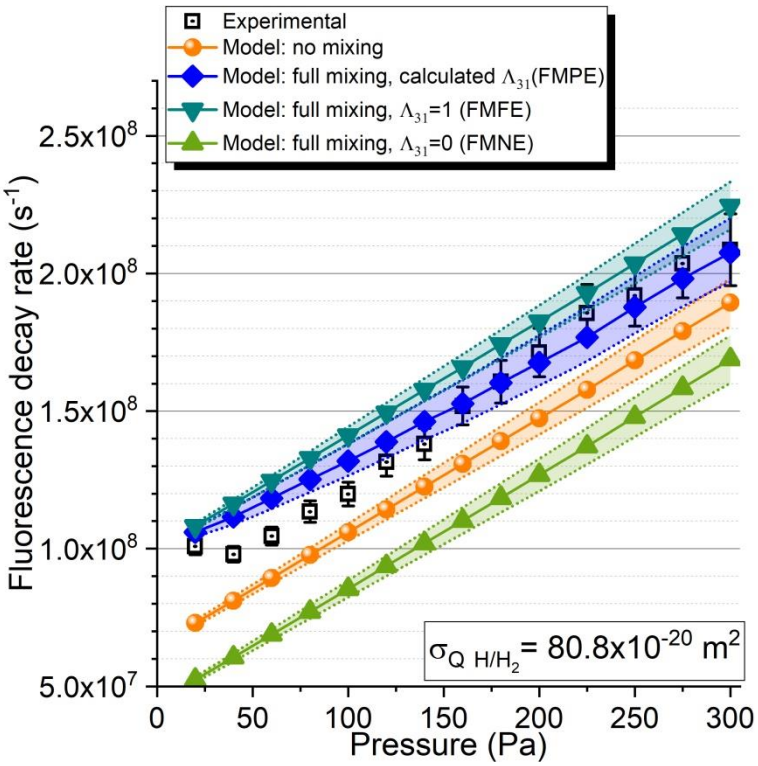

Figure 7 Comparison of experimental fluorescence decay rate of H(n=3) atoms with model predictions according to different scenarios, for $\sigma_{Q\,H(n=3)/H_2} = 80.8 \times 10^{-20}\ m^2$

4 Discussion

In this section, we discuss our results and the methodology adopted for the analysis of the de-excitation mechanisms of H(n=3) atoms in comparison with previously published data. In Table 1 are summarised the collisional quenching cross sections of H(n=3) atoms by H_2 molecules reported in this work and in several studies, including those where H atoms were produced either in a plasma [19], [20], [38], or by the interaction of H_2 molecules with an electron beam [39], and by photodissociation

of acetylene [41] or H_2 molecules [60]. The source of H atoms and the excitation pathways to the n=3 level, as well as the detection, the pressure range of colliders, are specified in the table.

Table 1 Collisional quenching of H(n=3) atoms by H_2 molecules

Authors	Source of atomic hydrogen	Excitation to H (n=3) level and detection	Detection of H_α fluorescence at 656.3 nm	H_2 pressure range (Pa)	A_3 ($10^7 s^{-1}$)	$\sigma_{Q\,H(n=3)/H_2}$ (Å^2 or 10^{-20} m^2)
Lewis and Williams [39] (1976)	Impact of 40 eV electrons with ground state H_2 molecules at room temperature	Electron-impact dissociative excitation of H_2 molecules	Time-integrated intensity with a spectrometer + PMT + photon counting apparatus	13 – 267		76
Catherinot and Dubreuil [38] (1978)	Positive column of a low-pressure H_2 glow discharge	LIF: excitation 2→3 with a tunable dye laser (4 ns).	Spectrometer + PMT	40 – 175	4.42±0.05	156±3
Meier *et al.* [19], Bittner *et al* [20] (1986, 1988)	He/H_2 microwave plasma.	TALIF: excitation 1s→3s, 3d with a dye laser	Filter + PMT	3 – 60 (H_2 partial pressure)	4.65 [19] 4.79 [20]	65±10 [20] [1)]
Preppernau *et al.*[41]	Photodissociation of acetylene at a pressure of 13 Pa using a dye laser beam at 205 nm	TALIF: excitation 1s→3s, 3d with a dye laser	Filter + PMT	3 – 1330		[2)]
Glass Maujean *et al.* [60]	Photodissociation of H_2 molecules by synchrotron radiation	Dissociative excitation of H_2 molecules to H(n=3)	Filter + PMT	1 – 15		40±18 (3s), 157±47 (3p), 57±10 (3d)[3)]
This work	Low-pressure H_2 microwave plasma	TALIF: excitation 1s→3s, 3d with a picosecond tunable laser	Filter + streak camera	20 – 300		90 – 106 (98±8)

1) *Cross section value reported by Bittner et al. [20] came from earlier measurements of $k_{Q\,H(n=3)/H_2}$ reported by Meier et al. [19] at room temperature. They found $k_{Q\,H(n=3)/H_2} = 1.99 \pm 0.30 \times 10^{-15}\ m^3 s^{-1}$*
2) *They found $k_{Q\,H(n=3)/H_2} = 1.78 \pm 0.14 \times 10^{-15}\ m^3 s^{-1}$ but the temperature was not determined and it was assumed this value was valid over a large temperature range from the ambient up to 3000 K*
3) *Cross section values reported were quoted for each individual level 3s, 3p or 3d, for a relative velocity of 5 km.s^{-1}*

In section 3.4, we determined the value of $\sigma_{Q\,H(n=3)/H_2}$ and compared experimental fluorescence decay rates with those predicted by the model, in reference to the values of $\sigma_{Q\,H(n=3)/H_2}$ published in [20], [38] that differ by a factor 2.4. Let us examine in more detail the assumptions made in their work and the methodologies chosen to extract collisional cross section values. This short review encompasses other works in the field, although we will mainly discuss the measurements reported in [19], [20] and [38].

Catherinot and Dubreuil investigated the fluorescence decay from H atoms in the n=3, 4 and 5 levels excited by laser absorption from the n=2 level [38]. Atoms were generated and excited to the n=2 level in a H_2 DC glow discharge generated in a capillary tube, where the pressure ranged from 40 to 175 Pa.

The population distribution in the 3s, 3p and 3d levels was assumed to follow the statistical distribution (i.e. full mixing). The laser excitation consisted of a single photon absorption from the n=2 level, which is different from the present study. They compared the intercept of their Stern-Volmer plot (A_3=4.42±0.05×10^7 s^{-1}) with values of total radiative radiative decay rate A_3 for the asymptotic cases $\Lambda_{31} = 1$ (9.98×10^7 s^{-1}) and $\Lambda_{31} = 0$ (4.41×10^7 s^{-1}), from which they concluded that the Lyman β line was totally trapped. They also investigated the variation of the fluorescence decay rate with plasma current intensity, interpreted as a variation of the H_2 molecular density with current, i.e. of the dissociation degree of the plasma with the electron density. Since they could not determine the atomic hydrogen densities directly, they combined these fluorescence decay measurements with electron density measurements, and built a model for estimating the dissociation degree of the plasma as a function of current and pressure [61]. In this way, they could determine a value of $156 \times 10^{-20}\ m^2$ for the quenching cross section $\sigma_{Q\ H(n=3)/H_2}$. They recognized that the cross section values they obtained for H(n=3, 4, 5) in collisions with H_2 molecules with such an indirect method are fairly high, especially when comparing with the values previously published by Lewis and Williams [39]. They attributed these differences to the possibility of a strongly enhanced quenching by the quasi metastable excited states ($c^3\Pi_u$ and $a^3\Sigma_g^+$) of H_2 that are readily produced in their capillary discharge, where they represent a rather large fraction, i.e. they suggest 5% of molecular hydrogen. This explanation would however result in a huge cross-section value, i.e. $700 \times 10^{-20}\ m^2$ [61], for the quenching of H(n=3) from the $c^3\Pi_u$ and $a^3\Sigma_g^+$ states of molecular hydrogen. Nevertheless, the interpretation of an enhanced quenching from H_2 excited states under plasma conditions remains fairly plausible if one considers not only the electronically excited states but also the vibrationally excited states that may significantly be populated under discharge conditions such as those investigated by Catherinot and Dubreuil [38], [61].

On the other hand, Meier *et al.* studied the collisional quenching of hydrogen, excited to the n=3 level by TALIF from the ground state, in collisions with small molecules (H_2, O_2, H_2O) and rare gases (He, Ar) [19]. Bittner *et al.* extended this study to the collisional quenching of H(n=3) by other molecules and rare gases (He, Ne, Kr, Xe) [20]. In these experiments, atomic hydrogen was produced in a He/H_2 plasma where the pressure was usually in the range 150 – 400 Pa, and the H_2 gas flow 2%. In order to investigate the collisional quenching of H(n=3) by molecular hydrogen, the H_2 partial pressure was varied in the range 3 – 60 Pa. Their measurements were performed in the flowing afterglow at a constant temperature value. The atomic hydrogen density in the afterglow was measured by NO_2 titration. Taking into account the quenching in collisions with helium atoms, which was usually negligible, they found $k_{Q\ H(n=3)/H_2} = 1.99 \pm 0.30 \times 10^{-15}\ m^3 s^{-1}$ at room temperature [19]. A value of $65 \pm 10 \times 10^{-20}\ m^2$ for $\sigma_{Q\ H(n=3)/H_2}$ was later reported by Bittner *et al.* [20]. Such value is 2.4 smaller than the value quoted by Catherinot and Dubreuil.

Meier *et al.* found an average radiative decay rate $A_3 = 4.65 \pm 0.32 \times 10^7 s^{-1}$ from their experiments with various quenchers, and concluded this value was in agreement with the statistical average radiative rate $A_{32} = 4.41 \times 10^7 s^{-1}$, which in other words corresponds to full mixing of the 3s, 3p and 3d levels with $\Lambda_{31} = 0$ (FMNE). Bittner *et al.* continued the analysis for other quenchers, and found an average radiative decay rate of $4.79 \pm 0.18 \times 10^7 s^{-1}$ from the intercept of their Stern-Volmer plots

acquired for various colliders [20]. They asserted that this value supports a predominant excitation of the 3d over the 3s state ($A_{3d\rightarrow 2p} = 6.47 \times 10^7 s^{-1}$) and reach the conclusion that collisional mixing is slow, which is exactly the opposite of Meier *et al.*'s conclusion.

A very close value of $2.04 \times 10^{-15}\ m^3 s^{-1}$ was determined for $k_{Q\ H(n=3)/H_2}$ at room temperature by Niemi *et al.* [28], under similar experimental conditions, namely TALIF measurements on atomic hydrogen in the flowing afterglow of a He/H_2 plasma, the H_2 partial pressure varying in the range 5 – 170 Pa. The atomic hydrogen densities were also determined in the afterglow by NO_2 titration. A value of $5.68 \times 10^7 s^{-1}$ was obtained for A_3 from the intercept of the Stern-Vomer plot, which they found consistent with the "no-mixing" scenario. They pointed out that it was impossible to conclude on the possibility of mixing amongst the 3s, 3p and 3d levels over the full pressure range of measurements, yet they still used the Stern Volmer approach, thus assuming a constant radiative decay rate, to determine collisional quenching coefficients.

The collisional mixing between the 3s, 3p and 3d levels was thoroughly investigated by Prepernau *et al.* [41] and Glass-Maujean *et al* [60]. In the latter study, separate collisional mixing and collisional quenching cross sections for the three sub-levels were derived from measurements described in reference [62], where atomic hydrogen was generated and excited through photodissociation of H_2 by synchrotron radiation in a gas cell at low pressures in the range 1 - 15 Pa. Starting from detailed rate equations describing the evolutions of 3s, 3p and 3d densities, Glass Maujean *et al.* approximated the solutions to this set of coupled rate equations by analytical functions, valid for low H_2 densities only, and fitted the modelled fluorescence signal to their experimental data to extract the various cross section values. In the range of pressures studied, where collisional quenching is still very moderate, collisional quenching cross sections derived from their analysis were given with high uncertainty, 45% for the 3s level and almost 30% for the 3p level. Preppernau *et al.* performed TALIF measurements on atomic hydrogen produced by the photodissociation of acetylene (pressure of 13 Pa) using a dye laser beam at 205 nm, in the presence of molecular hydrogen (3 to 1330 Pa) [41]. They showed that mixing of 3s, 3p and 3d levels is complete for H_2 partial pressures of a few tens of Pa. Further, Van der Heijden *et al.* [27] conducted TALIF measurements on atomic hydrogen in an expanding cascaded arc and obtained a full mixing of the 3s, 3p and 3d levels even for a molecular hydrogen partial pressure of 1.9 Pa. As they indicate, mixing between the H(n=3) sub-levels could be induced by local electric fields or by the laser beam electric field itself. Such mixing may actually be mediated by Stark mixing effects [63] under discharge conditions if large enough local electric fields are present in the discharge [64].

In any case, the assumption of no-mixing over all the pressure range investigated by Meier *et al.* (3-60 Pa) and Niemi *et al.* (5-170 Pa) is probably not valid. The erroneous interpretations of the measured fluorescence decay rates at low pressure by the different authors, arises as the radiative decay rate for no-mixing ($A_{3d\rightarrow 2p} = 6.47 \times 10^7 s^{-1}$) lies within the values for full mixing-full escape ($9.99 \times 10^7 s^{-1}$) and full mixing-no escape ($4.41 \times 10^7 s^{-1}$). In fact, the population distribution amongst the H(n=3) sub-levels and the subsequent radiative de-excitation kinetics are likely to change for the range of pressures considered in these studies. This means that the use of Stern-Volmer plots, that assume a

constant radiative decay rate, is questionable as shown by our picosecond TALIF measurements (cf. figure 3(b)).

The discussion above shows that determining the quenching cross section $\sigma_{Q\,H(n=3)/H_2}$ from Stern-Volmer plots under pressure conditions where the quenching rate remains small enough to enable using nanosecond TALIF is very difficult. Indeed under such conditions, i.e. typically pressure between few and 100 Pa, the atomic hydrogen TALIF process is affected by the mixing of the H(n=3) levels, that changes the radiative de-excitation kinetics, which results in a change of the radiative decay rate. Therefore, a major condition for the validity of the Stern-Volmer plot is not fulfilled. Surprisingly, this seems to have a limited consequence as far as cross section determination is concerned, at least for the conditions considered in this paper. Working at very low pressure in order to ensure a no-mixing regime and small enough quenching rate so as to use nanosecond TALIF is also difficult. The Stern-Volmer plots would indeed be performed using quite weak TALIF signal intensities (due to the low atomic densities) on a rather limited pressure range, which would result in a very large uncertainty. In order to use the Stern Volmer approach, one has to operate in a pressure range where full mixing has occurred and ignore the low pressure value in the plot. In such conditions, one has additionally to investigate whether the trapping of the Lyman β line, that may also affect the radiative decay rate, enters into the play. Our results show that this effect may substantially affect the value estimated for $\sigma_{Q\,H(n=3)/H_2}$ (cf. figures 6 and 7). In any case, it appears that for the discharge conditions investigated in this work and corresponding to atomic hydrogen densities of the order of $8 \pm 5 \times 10^{19}\ m^{-3}$ to $9 \pm 6 \times 10^{20}\ m^{-3}$, the Lyman β line is partially trapped, and taking into account the radiation trapping is essential for a satisfactory description of the fluorescence decay.

On the other-hand, one may design their experiments such that the Lyman β line is fully trapped and the radiative decay rate indeed becomes constant and therefore a Stern-Volmer plot can be used to determine the quenching cross-section values. However, these are favoured only at high-partial pressures of atomic hydrogen ($\Lambda_{31} \leq 0.1$ for atomic hydrogen densities greater than $4 \times 10^{23}\ m^{-3}$) where the overall fluorescence decay rate is greater than $1 \times 10^{9}\ s^{-1}$ (equivalent to $\tau_{fluo\,H}$ of 1 ns or less), and it would be necessary to use an ultra-fast laser coupled to a fast acquisition system.

The above discussion clearly highlights the problems that exist in the measurements of atomic hydrogen density using TALIF. Fortunately, our experiments involve picosecond-laser two-photon excitation and acquisition by a fast detector that allowed us to directly measure the fluorescence decay time and thereby directly measure the atomic hydrogen densities. However, in the absence of such advanced diagnostic tools, it is imperative to identify the correct regime of the depopulation processes of H(n=3). Fortunately, one will rarely encounter a no-mixing scenario for most conditions. However, the choice between FMFE, FMPE and FMNE depends on the optical thickness of the Lyman β line thus on the atomic hydrogen densities and the source length scale (laser beam radius). This means, it will be necessary to have a self-consistent approach to model the fluorescence decay rate and the atomic hydrogen densities.

5 Conclusion

In this study, we have investigated the depopulation mechanisms and kinetics of the H(n=3) level excited by two-photon absorption. Hydrogen atoms were produced in a H_2 microwave plasma operating in the pressure range 20-300 Pa. TALIF on atomic hydrogen was performed using a picosecond laser, and corresponding H(n=3) fluorescence signals were captured by a streak camera. Our experiments were combined with a depopulation model of H(n=3) that takes into account the mixing amongst the 3s, 3p and 3d levels and the subsequent Lyman β radiation trapping.

We showed how, under typical low pressure discharge conditions, the fluorescence decay rate used to determine the value of the quenching cross section $\sigma_{Q\,H(n=3)/H_2}$ of H(n=3) in collisions with H_2 molecules can be affected by the assumptions made on the mixing of H(n=3) sub-levels and the trapping of the Lyman β radiation under conditions typical for non-equilibrium plasmas.

The results obtained in this study clearly evidenced a full mixing amongst the H(n=3) sub-levels under discharge conditions, even at a pressure as low as 20 Pa. Whether this mixing is collisional or not is still an open question. It was also shown that in typical low-pressure non-equilibrium H_2 plasmas the radiative decay rate of H(n=3) can substantially vary with discharge conditions. If we take the example of the plasmas investigated in this work, the value of the Lyman β escape factor Λ_{31} is estimated close to 1 (0.94 – 0.98) at 20 Pa where the measured atomic hydrogen density is $\sim 8 \pm 5 \times 10^{19}\ m^{-3}$ and decreases down to 0.58 – 0.86 at 300 Pa, where the measured density is $\sim 9 \pm 6 \times 10^{20}\ m^{-3}$. As may be noticed, the accuracy on the estimates provided for the values of Λ_{31} is fairly limited and needs to be improved for a better description of the H(n=3) depopulation kinetics. Such an improvement would in fact require a full treatment of the radiative transport of the excitation.

The results summarised above show that the classical method based on the use of the Stern-Volmer plots to determine the quenching cross section $\sigma_{Q\,H(n=3)/H_2}$ becomes questionable. Therefore, we used two physics-based approaches to converge towards a range of possible values for the cross-section. The two methods yield similar although slightly different estimates of the quenching cross-section. Nevertheless, we would recommend a collisional quenching cross-section $\sigma_{Q\,H(n=3)/H_2}$ in the range $90 - 106 \times 10^{-20}\ m^2$ as determined from robust physical constraints on the variation of the escape factor with pressure. This recommendation translates to an average value of $98 \pm 8 \times 10^{-20}\ m^2$. When using TALIF with nanosecond-lasers or a slower acquisition system, it is absolutely necessary to correctly identify the depopulation regime in order to have accurate estimates of fluorescence decay times. Additionally, the substantially improved estimation of $\sigma_{Q\,H(n=3)/H_2}$ obtained in this work will be useful for the accurate estimation of H(n=3) fluorescence decay times and therefore the atomic hydrogen densities.

In the end, work is still required to improve the accuracy of atomic density measurements, especially there is a need to better quantify the ratio of the Kr and H two-photon excitation cross sections, since the only publication available to our knowledge [28] leads to a relative uncertainty of 50% on the atomic hydrogen density values.

6 Acknowledgements

This work was funded by the ANR ASPEN project (ANR-16-CE30-0004), the ANR ULTRAMAP project (ANR-20-CE51-0020) and the IDF regional project SESAME DIAGPLAS. One of the authors (Khaled Hassouni) acknowledges the support of the Institut Universitaire de France. The authors gratefully acknowledge G. A. Curley for helpful discussions and insightful advice.

7 References

[1] D. G. Goodwin, "Scaling laws for diamond chemical-vapor deposition. I. Diamond surface chemistry," *J. Appl. Phys.*, vol. 74, no. 11, pp. 6888–6894, Dec. 1993, doi: 10.1063/1.355063.

[2] A. Gicquel, F. Silva, and K. Hassouni, "Diamond Growth Mechanisms in Various Environments," *J. Electrochem. Soc.*, vol. 147, no. 6, p. 2218, Jun. 2000, doi: 10.1149/1.1393510.

[3] Z. Jia, Y. Fermi, A. Siby, O. Brinza, K. Hassouni, and S. Prasanna, "Enhanced gas-phase nucleation of diamond nanoparticles in a microplasma torch," *Plasma Process. Polym.*, p. e2200180, 2022, doi: 10.1002/PPAP.202200180.

[4] K. Pashova, I. Hinkov, X. Aubert, S. Prasanna, F. Bénédic, and S. Farhat, "Graphene synthesis by microwave plasma chemical vapor deposition: analysis of the emission spectra and modeling," *Plasma Sources Sci. Technol.*, vol. 28, no. 4, p. 045001, Apr. 2019, doi: 10.1088/1361-6595/AB0B33.

[5] P. Roca I Cabarrocas, "Plasma enhanced chemical vapor deposition of amorphous, polymorphous and microcrystalline silicon films," *J. Non. Cryst. Solids*, vol. 266–269, pp. 31–37, May 2000, doi: 10.1016/S0022-3093(99)00714-0.

[6] T. N.-M. Le, P. Raghunath, L. K. Huynh, and M. C. Lin, "A computational study on the adsorption configurations and reactions of SiH_x (x = 1-4) on clean and H-covered Si(100) surfaces," *Appl. Surf. Sci.*, vol. 387, pp. 546–556, Nov. 2016, doi: 10.1016/j.apsusc.2016.06.099.

[7] P. Sutter, J. Lahiri, P. Albrecht, and E. Sutter, "Chemical vapor deposition and etching of high-quality monolayer hexagonal boron nitride films," *ACS Nano*, vol. 5, no. 9, pp. 7303–7309, Sep. 2011, doi: 10.1021/nn202141k.

[8] J. H. Van Helden *et al.*, "Detailed study of the plasma-activated catalytic generation of ammonia in N_2-H_2 plasmas," *J. Appl. Phys.*, vol. 101, no. 4, p. 043305, Feb. 2007, doi: 10.1063/1.2645828.

[9] B. N. Bayer, P. J. Bruggeman, and A. Bhan, "Species, Pathways, and Timescales for NH_3 Formation by Low-Temperature Atmospheric Pressure Plasma Catalysis," *ACS Catal.*, pp. 2619–2630, Feb. 2023, doi: 10.1021/ACSCATAL.2C05492.

[10] K. Hassouni, S. Farhat, C. D. Scott, and A. Gicquel, "Modeling Species and Energy Transport in Moderate Pressure Diamond Deposition H_2 Plasmas," *J. Phys. III Fr.*, vol. 6, no. 9, pp. 1229–1243, Sep. 1996, doi: 10.1051/JP3:1996182.

[11] K. Hassouni, C. D. Scott, S. Farhat, A. Gicquel, and M. Capitelli, "Non-Maxwellian effect on species and energy transport in moderate pressure H_2 plasmas," *Surf. Coatings Technol.*, vol. 97, pp. 391–403, 1997.

[12] K. Hassouni, F. Silva, and A. Gicquel, "Modelling of diamond deposition microwave cavity generated plasmas," *J. Phys. D Appl. Phys.*, vol. 43, p. 153001, 2010, doi: 10.1088/0022-

3727/43/15/153001.

[13] J. C. Thomaz, J. Amorim, and C. F. Souza, “Validity of actinometry to measure N and H atom concentration in N_2-H_2 direct current glow discharges,” *J. Phys. D. Appl. Phys.*, vol. 32, no. 24, p. 3208, Dec. 1999, doi: 10.1088/0022-3727/32/24/317.

[14] A. Gicquel, M. Chenevier, K. Hassouni, A. Tserepi, and M. Dubus, “Validation of actinometry for estimating relative hydrogen atom densities and electron energy evolution in plasma assisted diamond deposition reactors,” *J. Appl. Phys.*, vol. 83, no. 12, p. 7504, 1998, doi: 10.1063/1.367514.

[15] W. G. Wang, Y. Xu, Z. C. Geng, Z. W. Liu, and A. M. Zhu, “Determination of atomic hydrogen density in non-thermal hydrogen plasmas via emission actinometry,” *J. Phys. D. Appl. Phys.*, vol. 40, no. 14, pp. 4185–4191, Jul. 2007, doi: 10.1088/0022-3727/40/14/013.

[16] U. Meier, K. Kohse-Hoinghaus, L. Schafer, and C.-P. Klages, “Two-photon excited LIF determination of H-atom concentrations near a heated filament in a low pressure H_2 environment,” *Appl. Opt.*, vol. 29, no. 33, p. 4993, Nov. 1990, doi: 10.1364/AO.29.004993.

[17] K. Niemi and T. Mosbach, “Is the flow tube reactor with NO_2 titration a reliable absolute source for atomic hydrogen ?,” vol. 367, no. 2, pp. 549–555, 2003.

[18] J. Bokor, R. R. Freeman, J. C. White, and R. H. Storz, “Two-photon excitation of the n = 3 level in H and D atoms,” *Phys. Rev. A*, vol. 24, no. 1, pp. 612–614, Jul. 1981, doi: 10.1103/PhysRevA.24.612.

[19] U. Meier, K. Kohse-Hoinghaus, and T. Just, “H and 0 atom detection for combustion applications: study of quenching and laser photolysis effects,” *Chem. Phys. Lett.*, vol. 126, no. 6, pp. 567–573, May 1986.

[20] J. Bittner, K. Kohse-höinghaus, U. Meier, and T. Just, “Quenching of two-photon-excited H(3s, 3d) and O(3p $^3P_{2,1,0}$) atoms by rare gases and small molecules,” *Chem. Phys. Lett.*, vol. 143, no. 6, pp. 571–576, Feb. 1988, doi: 10.1016/0009-2614(88)87068-4.

[21] J. Bittner, K. Kohse-Höinghaus, U. Meier, S. Kelm, and T. Just, “Determination of absolute H atom concentrations in low-pressure flames by two-photon laser-excited fluorescence,” *Combust. Flame*, vol. 71, no. 1, pp. 41–50, Jan. 1988, doi: 10.1016/0010-2180(88)90104-6.

[22] S. Agrup, F. Ossler, and M. Aldén, “Measurements of collisional quenching of hydrogen atoms in an atmospheric-pressure hydrogen oxygen flame by picosecond laser-induced fluorescence,” *Appl. Phys. B Lasers Opt.*, vol. 61, no. 5, pp. 479–487, 1995, doi: 10.1007/BF01081277.

[23] W. D. Kulatilaka, J. H. Frank, and T. B. Settersten, “Interference-free two-photon LIF imaging of atomic hydrogen in flames using picosecond excitation,” *Proc. Combust. Inst.*, vol. 32, pp. 955–962, 2009, doi: 10.1016/j.proci.2008.06.125.

[24] W. D. Kulatilaka, J. R. Gord, V. R. Katta, and S. Roy, “Photolytic-interference-free, femtosecond two-photon fluorescence imaging of atomic hydrogen,” *Opt. Lett.*, vol. 37, no. 15, p. 3051, Aug. 2012, doi: 10.1364/OL.37.003051.

[25] N. Lamoureux, K. K. Foo, and P. Desgroux, “Quantitative measurement of atomic hydrogen in low-pressure methane flames using two-photon LIF calibrated by krypton,” *Combust. Flame*, vol. 224, pp. 248–259, Feb. 2021, doi: 10.1016/j.combustflame.2020.12.010.

[26] P. Bletzinger and B. N. Ganguly, “High fractional dissociation efficiency in H a and H_2-N_2 gas mixtures in a helical resonator discharge,” 1995.

[27] H. W. P. van der Heijden, M. G. H. Boogaarts, S. Mazouffre, J. A. M. van der Mullen, and D. C. Schram, "Time-resolved experimental and computational study of two-photon laser-induced fluorescence in a hydrogen plasma," *Phys. Rev. E - Stat. Physics, Plasmas, Fluids, Relat. Interdiscip. Top.*, vol. 61, no. 4, pp. 4402–4409, 2000, doi: 10.1103/PhysRevE.61.4402.

[28] K. Niemi, V. Schulz-von der Gathen, and H. F. Dobele, "Absolute calibration of atomic density measurements by laser-induced fluorescence spectroscopy with two-photon excitation," *J. Phys. D. Appl. Phys.*, vol. 34, no. 15, pp. 2330–2335, 2001, doi: 10.1088/0022-3727/34/15/312.

[29] M. G. H. Boogaarts *et al.*, "Quantitative two-photon laser-induced fluorescence measurements of atomic hydrogen densities, temperatures, and velocities in an expanding thermal plasma," *Rev. Sci. Instrum.*, vol. 73, no. 1, p. 73, 2002, doi: 10.1063/1.1425777.

[30] M. Mrkvičková, J. Ráheľ, P. Dvořák, D. Trunec, and T. Morávek, "Fluorescence (TALIF) measurement of atomic hydrogen concentration in a coplanar surface dielectric barrier discharge," *Plasma Sources Sci. Technol.*, vol. 25, no. 5, p. 055015, Aug. 2016, doi: 10.1088/0963-0252/25/5/055015.

[31] J. B. Schmidt *et al.*, "Femtosecond, two-photon-absorption, laser-induced-fluorescence (fs-TALIF) imaging of atomic hydrogen and oxygen in non-equilibrium plasmas," *J. Phys. D. Appl. Phys.*, vol. 50, no. 1, p. 015204, Jan. 2017, doi: 10.1088/1361-6463/50/1/015204.

[32] S. Yatom, Y. Luo, Q. Xiong, and P. J. Bruggeman, "Nanosecond pulsed humid Ar plasma jet in air: shielding, discharge characteristics and atomic hydrogen production," *J. Phys. D. Appl. Phys.*, vol. 50, no. 41, Sep. 2017, doi: 10.1088/1361-6463/aa879c.

[33] Y. Yue, V. S. S. K. Kondeti, and P. J. Bruggeman, "Absolute atomic hydrogen density measurements in an atmospheric pressure plasma jet: generation, transport and recombination from the active discharge region to the effluent," *Plasma Sources Sci. Technol.*, vol. 29, no. 4, 2020, doi: 10.1088/1361-6595/ab7853.

[34] X. Yang *et al.*, "TALIF measurements of hydrogen and deuterium surface loss probabilities on quartz in low pressure high density plasmas," *Plasma Sources Sci. Technol.*, vol. 30, no. 1, p. 015013, Jan. 2021, doi: 10.1088/1361-6595/ABD454.

[35] L. Invernizzi *et al.*, "Peculiarities of measuring fluorescence decay times by a streak camera for ps-TALIF experiments in reactive plasmas," *Meas. Sci. Technol.*, vol. 34, no. 9, p. 095203, 2023, [Online]. Available: https://hal.science/hal-03886543.

[36] T. Holstein, "Imprisonment of Resonance Radiation in Gases," *Phys. Rev.*, vol. 72, no. 12, pp. 1212–1233, Dec. 1947, doi: 10.1103/PhysRev.72.1212.

[37] T. Holstein, "Imprisonment of Resonance Radiation in Gases. II," *Phys. Rev.*, vol. 83, no. 6, pp. 1159–1168, 1951.

[38] A. Catherinot, B. Dubreuil, and M. Gand, "Quenching of atomic states in a low-pressure hydrogen glow discharge," *Phys. Rev. A*, vol. 18, no. 3, pp. 1097–1102, 1978, doi: 10.1103/PhysRevA.18.1097.

[39] J. W. L. Lewis and W. D. Williams, "Collisional deactivation of atomic and molecular hydrogen," *J. Quant. Spectrosc. Radiat. Transf.*, vol. 16, no. 11, pp. 939–946, 1976, doi: 10.1016/0022-4073(76)90108-4.

[40] J. H. Tung, A. Z. Tang, G. J. Salamo, and F. T. Chan, "Two-photon absorption of atomic hydrogen from two light beams," *J. Opt. Soc. Am. B*, vol. 3, no. 6, pp. 837–848, 1986, doi: 10.1364/JOSAB.3.000837.

[41] B. L. Preppernau, K. Pearce, A. Tserepi, E. Wurzberg, and T. A. Miller, “Angular momentum state mixing and quenching of n=3 atomic hydrogen fluorescence,” *Chem. Phys.*, vol. 196, no. 1–2, pp. 371–381, Jun. 1995, doi: 10.1016/0301-0104(95)00086-4.

[42] W. L. Wiese and J. R. Fuhr, “Accurate atomic transition probabilities for hydrogen, helium, and lithium,” *J. Phys. Chem. Ref. Data*, vol. 38, no. 3, pp. 565–719, 2009, doi: 10.1063/1.3077727.

[43] R. Mewe, “Relative intensity of helium spectral lines as a function of electron temperature and density,” *Br. J. Appl. Phys.*, vol. 18, no. 1, pp. 107–118, 1967, doi: 10.1088/0508-3443/18/1/315.

[44] F. E. Irons, “The escape factor in plasma spectroscopy-I. The escape factor defined and evaluated,” *J. Quant. Spectrosc. Radiat. Transf.*, vol. 22, no. 1, pp. 1–20, Jul. 1979, doi: 10.1016/0022-4073(79)90102-X.

[45] F. E. Irons, “The escape factor in plasma spectroscopy-II. The case of radiative decay,” *J. Quant. Spectrosc. Radiat. Transf.*, vol. 22, no. 1, pp. 21–36, 1979, doi: 10.1016/0022-4073(79)90103-1.

[46] E. Bisceglia, “Enhancement of nitrogen atom density using microwave pulsed discharges. Methodology combining laser-induced fluorescence and collisional-radiative model.,” Université Sorbonne Paris Nord, 2021.

[47] I. I. Sobel’man, L. A. Vainshtein, and E. A. Yukov, *Excitation of Atoms and Broadening of Spectral Lines*, 1995th ed. Springer Verlag, Berlin, 1995.

[48] H. R. Griem, *Spectral Line Broadening by Plasmas*. New York: Academic Press, 1974.

[49] A. C. G. Mitchell and M. W. Zemansky, *Resonance radiation and excited atoms*, 1961st ed. The syndics of the Cambridge University press, 1934.

[50] E. Tiesinga, P. J. Mohr, D. B. Newell, and B. N. Taylor, “CODATA Recommended Values of the Fundamental Physical Constants: 2018,” *J. Phys. Chem. Ref. Data*, vol. 50, no. 3, Sep. 2021, doi: 10.1063/5.0064853.

[51] T. Prohaska *et al.*, “Standard atomic weights of the elements 2021 (IUPAC Technical Report),” *Pure Appl. Chem.*, vol. 94, no. 5, pp. 573–600, May 2022, doi: 10.1515/pac-2019-0603.

[52] F. Brouillard *et al.*, “Associative Ionisation in Low Energy Collisions,” *Phys. Scr.*, vol. T96, no. 1, p. 86, 2002, doi: 10.1238/Physica.Topical.096a00086.

[53] E. Bisceglia *et al.*, “Investigation of N(4S) kinetics during the transients of a strongly emissive pulsed ECR plasma using ns-TALIF,” *Plasma Sources Sci. Technol.*, vol. 30, no. 9, Sep. 2021, doi: 10.1088/1361-6595/AC0DA1.

[54] K. Gazeli, X. Aubert, S. Prasanna, C. Y. Duluard, G. Lombardi, and K. Hassouni, “Picosecond two-photon absorption laser-induced fluorescence (ps-TALIF) in krypton: The role of photoionization on the density depletion of the fluorescing state Kr $5p'[3/2]_2$,” *Phys. Plasmas*, vol. 28, no. 4, Apr. 2021, doi: 10.1063/5.0041471.

[55] K. Gazeli, G. Lombardi, X. Aubert, and C. Y. Duluard, “Progresses on the Use of Two-Photon Absorption Laser Induced Fluorescence (TALIF) Diagnostics for Measuring Absolute Atomic Densities in Plasmas and Flames,” pp. 145–171, 2021.

[56] S. A. Astashkevich *et al.*, “Radiative characteristics of 3p Σ, Π; 3d Π−, Δ− states of H_2 and determination of gas temperature of low pressure hydrogen containing plasmas,” *J. Quant. Spectrosc. Radiat. Transf.*, vol. 56, no. 5, pp. 725–751, Nov. 1996, doi: 10.1016/S0022-

4073(96)00103-3.

[57] M. Osiac, B. P. Lavrov, and J. Röpcke, “Intensity distributions in R and P branches of (0–0) band of the $A^1\Pi \rightarrow X^1\Sigma^+$ electronic transition of the BH molecule and determination of gas temperature in non-equilibrium plasmas,” *J. Quant. Spectrosc. Radiat. Transf.*, vol. 74, no. 4, pp. 471–491, Aug. 2002, doi: 10.1016/S0022-4073(01)00268-0.

[58] L. Tomasini, A. Rousseau, G. Gousset, and P. Leprince, “Spectroscopic temperature measurements in a H_2 microwave discharge,” *J. Phys. D Appl.*, vol. 29, pp. 1006–1013, 1996.

[59] K. Dzierżęga, U. Volz, G. Nave, and U. Griesmann, “Accurate transition rates for the 5 p − 5 s transitions in Kr I,” *Phys. Rev. A*, vol. 62, no. 2, p. 022505, Jul. 2000, doi: 10.1103/PhysRevA.62.022505.

[60] M. Glass-Maujean, S. Lauer, H. Liebel, and H. Schmoranzer, “Collisional quenching of the H(n = 3) atoms by molecular hydrogen: cross section measurements,” *J. Phys. B At. Mol. Opt. Phys.*, vol. 33, pp. 4593–4601, 2000, doi: 10.1088/0953-4075/33/21/305.

[61] B. Dubreuil and A. Catherinot, “Étude d’une décharge luminescente d’hydrogène par perturbation laser : relaxations atomique et moléculaire, équilibre de dissociation,” *J. Phys.*, vol. 39, no. 10, pp. 1071–1084, Oct. 1978, doi: 10.1051/jphys:0197800390100107100.

[62] S. Lauer *et al.*, “Collisional quenching of H(3 l) atoms by molecular hydrogen,” *J. Phys. B At. Mol. Opt. Phys.*, vol. 31, no. 13, pp. 3049–3056, Jul. 1998, doi: 10.1088/0953-4075/31/13/021.

[63] M. Glass-Maujean, “Measurement of the $3^2S_{1/2}$-$3^2D_{3/2}$ and $3^2S_{1/2}$-$3^2D_{5/2}$ intervals in atomic hydrogen,” *Opt. Commun.*, vol. 8, no. 3, pp. 260–262, Jul. 1973, doi: 10.1016/0030-4018(73)90142-9.

[64] D. Vrinceanu and M. R. Flannery, “Classical and quantal collisional Stark mixing at ultralow energies,” *Phys. Rev. A - At. Mol. Opt. Phys.*, vol. 63, no. 3, pp. 1–22, 2001, doi: 10.1103/PhysRevA.63.032701.